Continental Shelf Research 54 (2013) 1–13

Contents lists available at SciVerse ScienceDirect

Continental Shelf Research

journal homepage: www.elsevier.com/locate/csr

Characterizing the effluence near Waikiki, Hawaii with a coupled biophysical model

Abby E. Johnson, Brian S. Powell *, Grieg F. Steward

School of Ocean and Earth Science and Technology, University of Hawaii, Manoa. 1000 Pope Rd., Honolulu, HI 96822, USA

ARTICLE INFO

Article history:
Received 12 May 2012
Received in revised form
5 September 2012
Accepted 18 December 2012
Available online 4 January 2013

Keywords:
Coupled biophysical model
Physical forcing
Enterococcus spp.
Plume dynamics

ABSTRACT

Aperiodic discharge from the Ala Wai Canal near Waikiki, Hawaii is often contaminated with naturally occurring harmful bacteria that may affect nearby beaches. Using a coupled hydrodynamic and biological model, we examine how tides, wind, surface waves, and light affect the fate of this effluent plume. The nearshore circulation and tidal flows constrain the freshwater plume to the surface. Winds can overcome both the stratification and ambient tidal advection to keep the plume to the west (away from major beaches) and mix the plume deeper into the water column. Surface waves due to swell act to mix the plume deep and keep the plume onshore. We find that the plume does not extend offshore in the presence of winds or waves. Using *Enterococcus* spp. as the bacterial agent, we find that residency is increased when mixed deeper away from the light. Comparing predicted *Enterococcus* spp. with in-situ samples for five distinct plume events, we find that the model accurately represents the observed bacterial concentrations when the Ala Wai is the primary source of *Enterococcus* spp. discharge. The results show that predictive models may be an invaluable complement to water quality sampling programs for regions of high human activity.

1. Introduction

Freshwater plumes are a source of sediments, nutrients, and pollutants into the ocean that affect nearshore coastal waters (Masse and Murthy, 1992). Nearshore physical forcings (e.g., ambient flow, wind, tides, and waves) are critical to characterizing the dynamics of these plumes. Numerous studies have been conducted to better understand how plumes disperse upon entering the coastal ocean (Garvine, 1995; Hickey et al., 1998; Orton and Jay, 2005). Modeling studies (O'Donnell, 1990; Wiseman and Garvine 1995; Berdeal et al., 2002; Choi and Wilkin, 2007) have helped to parameterize the effects of wind, tides, and bathymetry on the evolution of persistent large-scale plumes, but the combined effects of wind, tides, wave forcing on the plume physics and their impact along with UV effects on bacterial concentrations remain poorly constrained.

Numerical simulations have been used to characterize freshwater coastal plumes, but the focus has been on high-volume plumes with large Kelvin numbers, K (see Garvine 1987, 1995; O'Donnell, 1990; Wiseman and Garvine, 1995). The Kelvin number is determined by the ratio of the plume channel width to the Rossby radius and measures the importance of earth rotation (Wiseman and Garvine, 1995). Plumes with $K \geq 1$ are large volume and affected by Earth's rotation on long time-scales, while those with a small K (<1) are quickly incorporated into the ambient flow (Garvine, 1987 and 1995; O'Donnell, 1990).

Tidal forcing strongly influences both small and large-scale coastal plumes. Examples include the small-scale Connecticut River plume, which has a flow direction that varies with tidal phase (Whitney and Garvine, 2006). Using a numerical model, Guo and Valle-Levinson (2007) analyzed tidal effects on an outflow plume in Chesapeake Bay and concluded that a bottom-advected plume occurred due to tidal forcing; whereas, a surface-advected plume developed without tidal forcing. For the high-volume Columbia River plume, plume mixing was strongest near a tidal front, with high nutrient and sediment exchange (Orton and Jay, 2005).

Wind forcing has the potential to influence the advection, mixing, and transport of river plumes. The effects of wind forcing have been examined primarily for freshwater plumes with large K values. Choi and Wilkin (2007) showed that wind forcing affected the amount of discharge and the trajectory of the surface-advected Hudson River plume. For a high-discharge event without wind forcing, the plume formed a large recirculating bulge of freshwater outside the river mouth. Southward winds advected the plume to the south and northward wind advected the plume offshore and along the Long Island coast. Hickey et al. (1998) and Berdeal et al. (2002) found that the Columbia River plume

* Corresponding author. Tel.: +1 808 956 6724.
E-mail address: powellb@hawaii.edu (B.S. Powell).

0278-4343/$ - see front matter © 2013 Elsevier Ltd. All rights reserved.
http://dx.doi.org/10.1016/j.csr.2012.12.007

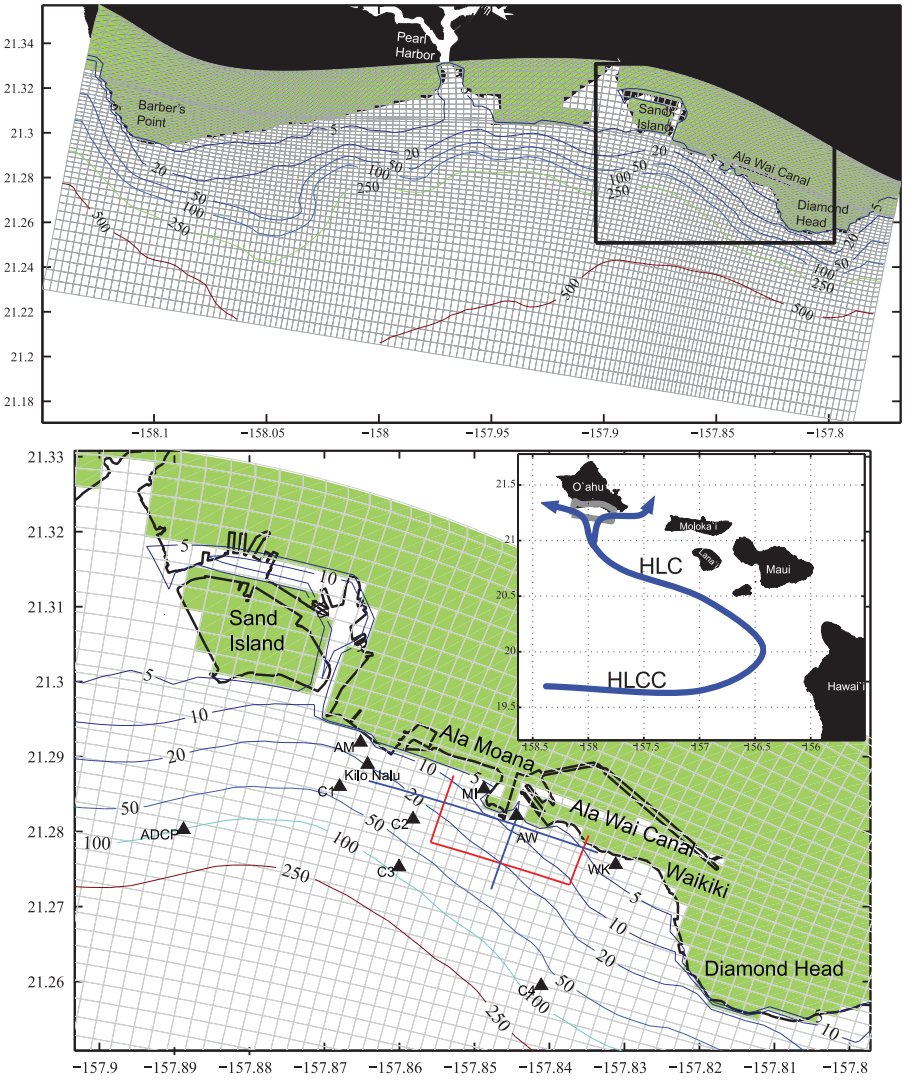

Fig. 1. Map and model grid of the O'ahu study. The upper panel shows the study region of Mamala Bay along the southern coast of O'ahu. Inset figure shows several islands of the Hawaiian chain along with the primary mean currents of the region. The inset grey box outlines the model domain, which includes southern Oahu and Mamala Bay. The lower panel focuses upon the Ala Wai region. The model grid and landmask are shown with the known coastline data plotted in black. The modeled Ala Wai canal is along a grid row for finite-differencing. The observed station locations and analysis transect lines from the results are shown. (For interpretation of the references to color in this figure legend, the reader is referred to the web version of this article.)

responded to wind forcing within hours and moved offshore with southward, upwelling winds that tend to occur during the summer and moved onshore during northward, downwelling winds that occur in the winter. Downwelling-favorable winds can also create vertical mixing that deepen freshwater plumes (Pullen and Allen, 2000).

Each of these studies were of river systems with high volume, steady discharge. In this study, we investigate rain-driven, effluent plumes from the Ala Wai Canal, a small artificial estuary with an outlet adjacent to the beaches at Waikiki in Honolulu, Hawaii (Fig. 1). Since the canal was built, its water quality has deteriorated such that it can be a public health risk (Venzon, 2007), and it has been found to be a source of *Enterococcus* spp. contamination on nearby beaches (Connolly et al., 1999); although, it is not a source of sediments or terrestrial nutrients. Due to infection risks associated with plume events, a predictive tool of plume evolution would be desirable for civil planning purposes and could improve assessment risks to beachgoers. Notably, a causal correlation between *Enterococcus* spp. abundance in near-shore waters, inferred from extinction culturing, and episodic rainfall events has been established (Hamilton et al., 1995; Connolly et al., 1999); however, a mechanistic understanding of the specific contribution of the plume from the Ala Wai Canal is lacking.

We examine the impacts of physical forcing on the Ala Wai plume, which we characterize as an aperiodic, low *K*, freshwater, effluent plume from a small canal into a reef-protected surf zone. Our aim is to determine what controls the fate of the harmful bacteria released into the coastal zone, and particularly the conditions that cause the plume to impact Waikiki to the southeast. We present the use of a biological model of *Enterococcus* spp. nested in a high-resolution numerical circulation model to examine the effects of ambient flow, wind, tides, and waves on a low-volume freshwater plume.

2. Methods

2.1. ROMS

We use Regional Ocean Modeling System (ROMS) to characterize the circulation of the south coast of Oahu during large plume discharge from the Ala Wai Canal triggered by rain events.

ROMS is a high-resolution, hydrostatic, free-surface, terrain-following vertical coordinate primitive equation ocean model. Momentum is solved using a split-explicit time-stepping scheme and coupling between barotropic and baroclinic modes (Shchepetkin and McWilliams, 2005). The resolution of our model grid is variable, ranging from 66 m cross-shore resolution at the shore to 575 m in the deep water offshore with 20 vertical s-layers. The grid covers the south shore of Oahu from Diamond Head to Barber's Point, known as Mamala Bay, and includes the Ala Wai Canal, Keehi Lagoon, and entrance to Pearl Harbor. The grid extends approximately 15.5 km offshore as shown by the inset of Fig. 1. Because ROMS is a finite-difference C-grid model, the Ala Wai Canal is represented slightly differently than the actual canal which varies in its direction. The represented volume and depths of the canal match well with the true canal.

The grid used for this study is one-way nested within two outer model grids. The middle grid (not shown in the figure) comprises all of the island of Oahu as well as the western portion of the island of Molokai. The middle grid is nested within an outer-most grid (not shown), which covers all of the major Hawaiian Islands and has been used for a number of studies of the region (Janekovic and Powell, 2012; Matthews et al., 2012; Powell et al., 2012; Natarov and Powell, 2012). The 1/8° resolution Navy Coastal Ocean Model (Barron et al., 2006) provides the boundary conditions for the outer-most grid. All models were integrated from 2004 through 2010.

For each plume event, the model was integrated for twelve different configurations to quantify the effects of the physical forcing as listed in Table 1. Ala Wai discharge events are connected to strong rain storms on the island of Oahu and tend to last for no more than two days. To examine the effects of these discrete discharge events, each experiment spans a two week time period surrounding the event. Using an average Intel-based machine with 32 CPU cores, each two week integration requires less than 30 min to execute. The outer-model grids are integrated with all physical forcing except waves to provide boundary conditions for the grid used in this study. For experiments without tidal forcing, boundary conditions are detided to eliminate barotropic and baroclinic tides. This ensures consistent low-frequency dynamics between all configurations.

All experiments include the inertial circulation of Mamala Bay, which is provided by the outer-model. The mean flow off the south shore of Oahu is controlled by the Hawaii Lee Current (HLC), which is the westward return branch of the Hawaiian Lee Counter Current (HLCC). Due to wind stress patterns behind the Big Island of Hawaii, the HLCC is formed and flows west to east (Xie et al., 2001). The HLCC turns and flows along the leeward side of the island chain forming the HLC. South of Oahu, the HLC produces an onshore flow that bifurcates in Mamala Bay (see inset of Fig. 1), forming a mean eastward current offshore of the Ala Wai Canal (Hamilton et al., 1995).

Table 1
Experiment names for differing combinations of forcing.

Experiment name	Wind forcing	Tidal forcing	Average wave forcing	Maximum wave forcing
NOFRC				
WFRC	X			
TFRC		X		
WTFRC	X	X		
AFRC			X	
WAFRC	X		X	
TAFRC		X	X	
WTAFRC	X	X	X	
MFRC				X
WMFRC	X			X
TMFRC		X		X
WTMFRC	X	X		X

W designates. Wind, *T* for tidal, *A* for average wave, and *M* for maximum wave forcing. NOFRC designates the ambient circulation without forcing.

We compare the model currents with an acoustic Doppler current profiler (ADCP) deployed 2.5 km offshore of Sand Island (see ADCP marker on Fig. 1) during 2007. Daily averages (not decided) of modeled and observed velocities were oriented into alongshore and cross-shore directions and the time-means at each depth were compared. The model captures the amplitude and two-layer structure of the observed mean flow, with eastward flows ranging from 0.1 to 4.2 cm s^{-1} above 45 m depth and westward flows ranging from 0.7 to 4.1 cm s^{-1} below 45 m. These mean velocities are misleading as they average out the strong alternating flow of the tidal cycle, which is as large as 18 cm s^{-1}. The average modeled alongshore currents were slightly stronger by 0.2 to 1.3 cm s^{-1} than the observed currents. The modeled cross-shore currents were slightly weaker (0.1 to 0.2 cm s^{-1}) than observed above 25 m depth, and slightly stronger below 25 m. Root mean square (RMS) values of the model minus observed residual currents ranged from 0.43 to 0.84 cm s^{-1} for alongshore currents, and 0.09–0.76 cm s^{-1} for cross-shore currents for all available times including the tidal variation. Given that the flow may vary between $+/-$ 18 cm s^{-1} over a tidal cycle, these comparisons suggest that the model gives a realistic depiction of the mean ambient flow in Mamala Bay.

Atmospheric forcing for the model is provided by a regional weather research and forecasting (WRF) model with 1.5 km resolution. Surface wind stress is prescribed via the Coupled Ocean-Atmosphere Response Experiment (COARE) flux algorithm (Fairall et al., 1996). The dominant winds for the Hawaiian Islands are the Trade winds that blow from the northeast to the southwest. From October to April it is common for the Trade winds to weaken and for southerly storm winds (known as Kona winds) to impact the south shore of Oahu. To examine the influence of local wind forcing on the plume, the wind forcing is set to zero for some experiments (downwelling heat fluxes and precipitation fluxes remain unchanged) while maintaining the ambient flow, which may include a regional wind-driven component.

Tidal forcing, which includes barotropic and baroclinic tides, is imposed through the boundary conditions from the parent grid (Janekovic and Powell, 2012) to examine the impact on the plume. The Oregon State University TOPEX/POSEIDON Global Inverse Solution (TPXO) provides barotropic tidal forcing to the outer-most model (Egbert et al., 1994). Conversion from the barotropic to baroclinic tides occurs along the steep ridges of the model (Carter et al., 2008; Powell et al., 2012). The alongshore coastal currents in Mamala Bay are dominated by the tides, primarily the semidiurnal M_2 constituent (Hamilton et al., 1995; Eich et al., 2004; Alford et al., 2006). For the semidiurnal barotropic tide, currents generally are oriented along isobaths with some amplification around headlands, such as Diamond Head. For the semidiurnal baroclinic tide, ~60% of the current variability in the bay is coherent with the barotropic tide, with a dominant alongshore component that exhibits a two-layer depth structure (Eich et al., 2004). The remainder of the variability is incoherent and difficult to characterize accurately in model simulations. In our model simulations, 70% of the nearshore current variance at the Ala Wai Canal is due to the barotropic tide, and the majority (97.5%) of that variance is in the alongshore direction. During ebb tide the flow is to the east towards sampling station WK, and during flood tide the flow is to the west towards sampling station AM.

Surface wave forcing is included in some experiments to examine its effects on the plume. Wave conditions are specified based on the U.S. Army Corps of Engineers (USACE) Wave Information Studies product, which estimates past wave conditions using a global spectral wave model (WAVEWATCH III) with

observed winds. The average and maximum south swell conditions were taken at the closest synthetic buoy located southwest of the island of Oahu. A high-resolution (~20 m) wind-wave model (WWM) (Roland et al., 2009) with high-resolution bathymetry from the Hawaii Mapping Research Group was used to create a spectral representation of these wave conditions along the south shore of Oahu. The significant wave height for the average south swell conditions was 1.34 m with a period of 13.28 s. For maximum south swell conditions (defined as 90th percentile of recorded wave heights and period from WAVEWATCH III) the significant wave height was 1.67 m at a period of 13.85 s. Both swell conditions propagated from 190° (nearly from the south). The output of the WWM was used to generate significant wave height, period, wavelength, and direction forcings for each point of the ROMS grid providing a complex surface wave field to best approximate the south shore.

The model domain contains an Ala Wai Canal with realistic length, width, and depth, based on multibeam bathymetry data obtained from the Hawaii Ocean Observing System. To simulate Ala Wai Canal plume rates, we use streamflow time series obtained from the United States Geological Survey (USGS) for the Manoa–Palolo drainage canal, which accounts for nearly 70% of the total freshwater input to the Ala Wai Canal. Mean stream gauge flow was $0.55 \pm 2.3\ m^3\ s^{-1}$ between 2004 and 2009. Rain events described in this manuscript were chosen to represent large events (> 99.99th percentile of 15 min interval stream gauge readings). Because there is no monitoring of other source inputs into the Ala Wai Canal, the Manoa–Palolo stream gauge data were increased by 30% to account for the other missing inputs, including drainage canals, surface runoff, etc. The adjusted streamflow data were used as point source forcing within ROMS, with a salinity of 2 psu and temperatures that matched ambient conditions. *Enterococcus* spp. is treated as a passive tracer in the hydrodynamic model.

2.2. Biological model

For this study, we use a biological model to examine the role of light in the time evolution of *Enterococcus* spp. The biological model, integrated at each time-step with the circulation model, is based upon the ultra-violet (UV) decay model from Hassen et al. (2000):

$$\frac{dN}{dt} = -kI_{UV}N, \tag{1}$$

where k ($m^2\ W^{-1}\ day^{-1}$) is the UV inactivation coefficient for *Enterococcus* spp., I_{UV} is the intensity of UV irradiation ($W\ m^{-2}$), and N is the concentration of Enterococcus spp. ($nmol\ m^{-3}$). k is strain-specific, and bacteria resistant to UV irradiance are characterized by low k. We choose k equal to that detailed in Davies-Colley et al. (1994) who found that only 10% of *Enterococcus* spp. is viable after 81 min exposure from experiments with mid-day irradiances of $1200\ W\ m^{-2}$.

As *Enterococcus* spp. distributions are not restricted to the surface layer, we must determine the average diffuse attenuation coefficient, a in m^{-1}, for light penetration in coastal tropical waters for Mamala Bay. The solar irradiance in water decays exponentially with depth:

$$\frac{dI}{dz} = -aI(0), \tag{2}$$

where $I(0)$ is the solar irradiance at the surface that is prescribed by the atmospheric model, z is depth, and a is the spectral attenuation coefficient (Parsons et al., 1977). Connolly et al. (1999) computed the attenuation coefficient at the 10 m isobath in Mamala Bay and found an average decay rate of $0.212\ m^{-1}$. UV irradiance is the primary spectral band that causes inactivation (loss of culturability) in bacteria, but makes up less than 10% of the total solar irradiance, so the penetrating irradiance is scaled appropriately to approximate I_{UV}.

Blue light (475 nm), which accounts for 0.5% of the total solar radiation, is the photoreactivation band (Hassen et al., 2000). Photoreactivation is the ability of micro-organisms to repair UV damaged DNA. We use the attenuated irradiance from (2) to approximate the blue light irradiance, I_b. The full biological model with reactivation is given by:

$$\frac{dN(z)}{dt} = -kI_{UV}(z)N(z) + pI_b(z)N(z), \tag{3}$$

where p is the growth coefficient due to photoreactivation.

Initially, *Enterococcus* spp. is used as a passive tracer with the biological decay model disabled to determine the effects of the physical forcing from ambient flow, wind, tides, and waves. We identify the plume by waters that meet or exceed a single-sample maximum of 100 CFU of *Enterococcus* $100\ mL^{-1}$ as established by Hawaii's Department of Health for acceptable water quality.

3. Results and discussion

3.1. Effects of forcing

We performed a detailed analysis of five plume events and present two illustrative plumes (Table 2). Event 1 began on 11 December, 2008 at 10:00 HST. Due to heavy rains, the Manoa–Palolo

Table 2
Description and summary of conditions for five plume events from the. Ala Wai Canal.

Event name	OCT05* (Event 2)	MAR06	NOV07	DEC08* (Event 1)	MAR09
Period:					
Start	10/16/05	3/14/06	10/29/07	12/3/08	3/6/09
End	11/1/05	4/2/06	11/12/07	12/22/08	3/23/09
Peak ($m^3\ s^{-1}$)					
Streamflow:	125.5	188.8	37.99	101.5	117.2
Date–time:	10/25–1 am	3/22–1 am	11/4–8 am	12/11–10 am	3/14–5 am
Peak ($m^3\ s^{-1}$)					
Plume:	−55.56	−70.91	−22.05	−72.16	−44.15
Date–time:	10/25–2 am	3/23–10 pm	11/4–8 am	12/11–12 pm	3/14–6 am
Wind (from) direction	NE	S	E/NE	SE	E/NE
Average wind speed ($m\ s^{-1}$)	5.11	3.5606	3.75	6.14	1.79
Tidal amplitude (cm)	30	60	55	70	55
Mean near-shore flow direction	West	West	East	East	West
Maximum plume area (m^2)	1.5×10^7	3.2×10^7	9.1×10^6	9.0×10^6	1.87×10^7
Maximum plume depth (m)	5	8	5	9	4

* events are presented in detail in the Results and Discussion section.

stream gauge recorded a peak streamflow of 73.1 $m^3 s^{-1}$. The model peak streamflow was 101.5 $m^3 s^{-1}$ (recall observed streamflows were increased by 30%). This caused a plume event from the Ala Wai Canal with a peak ocean discharge around 12:00 HST, and was followed by a second peak streamflow of 46.8 $m^3 s^{-1}$ on the evening of 13 December that caused a continual modeled plume until the morning of 16 December. During Event 1, there were strong Kona winds that blew from the southeast to the northwest with an average speed of 6.14 ± 1.95 m s^{-1}, and the peak model discharge occurred during spring tide with tidal amplitudes near 70 cm.

We compared this with Event 2 which occurred in October, 2005. The model plume began to flow out of the Ala Wai Canal on 23 October at 08:00 HST and lasted until the evening of the 26th. On 25 October, 2005 at 01:00 HST, the model peak streamflow of 125.5 $m^3 s^{-1}$ was preceded by a plume 90% smaller two days earlier. Both rain events caused a continual plume to occur from the Ala Wai Canal with a modeled peak ocean discharge on 25 October at 01:00 HST. Modeled Trade winds had a mean speed of 5.11 ± 1.36 m s^{-1}, and the maximum plume was during a neap tide with an amplitude of approximately 30 cm.

We begin our description of the forcing effects on the plumes by considering the total plume surface area (above the health advisory limit) as a function of time. We use surface area in a manner similar to Walker (1996) and Fong and Geyer (2001). For both events, the plume surface areas were largest for the ambient (NOFRC) and tidal forcing (TFRC) cases (Fig. 2). For Event 1, mean ambient nearshore circulation was to the east with magnitudes ranging from 10 to 20 cm s^{-1}, causing net eastward advection of the plume for the NOFRC case; however, a portion of the plume dispersed both offshore and to the west (Fig. 3a). For Event 2, the small plume preceding the primary plume combined with a weak mean circulation to the west spreading the plume outward (Fig. 3d). Tidal forcing caused the plume to oscillate alongshore to the east on an ebb tide and to the west on a flood tide, which also resulted in the plume having a large surface area for both events. Surface areas were significantly reduced when including wind forcing (WFRC) or maximum wave forcing (MFRC) experiments. For these comparisons, the differences between the MFRC and average wave forcing (AFRC) experiments were not significant, and we will focus on the MFRC results. In response to the direction of the waves and the mixing that occurred, the surface area of the MFRC plume was reduced by 41% for Event 1 and 75% for Event 2 compared to the NOFRC case. For the WFRC experiments surface areas were reduced by 31% for Event 1 and 85% for Event 2 (Fig. 2).

Because the discharges are caused by aperiodic rain events, the plume is freshwater with a modeled salinity of 2. Tomlinson et al. (2011) observed similar salinities in the buoyant surface waters of the Ala Wai Canal during rain events. Freshwater plumes from the Ala Wai are buoyant with an average depth of 0.5 m, except in areas where forcing mixed the plume deeper, so we focused on maximum depths. For both events, the modeled plumes reached maximum depths of approximately 1 m for the NOFRC and TFRC cases because neither the ambient flow or tidal forcing were able to overcome the density stratification of the freshwater lens to mix the plume deeper (Fig. 4). The magnitude of the wind caused the plume to mix to greater depths for Event 1 (Fig. 4a). Kona wind speeds increased the morning of 10 December and reached 10.3 m s^{-1} by late on 11 December causing the plume to be forced onshore and to the west extending past Sand Island into a deep lagoon where it mixed to depths of 4.4 m. For Event 2, the depth of the plume was not increased for the WFRC case compared to the NOFRC case because of a lower peak wind speed of 6.2 m s^{-1} (Fig. 4b). Plumes reached the greatest depths for experiments with wave forcing. For Event 1, the mean circulation remained to the east with wave forcing, which forced the plume onto Waikiki beaches (Fig. 3c). Increased significant wave height was found in the model within the Waikiki bight showing that waves propagating from the south-southwest break upon entering the Waikiki bight causing the plume to mix to maximum depths of 5.5 m. For Event 2, the mean circulation remained to the

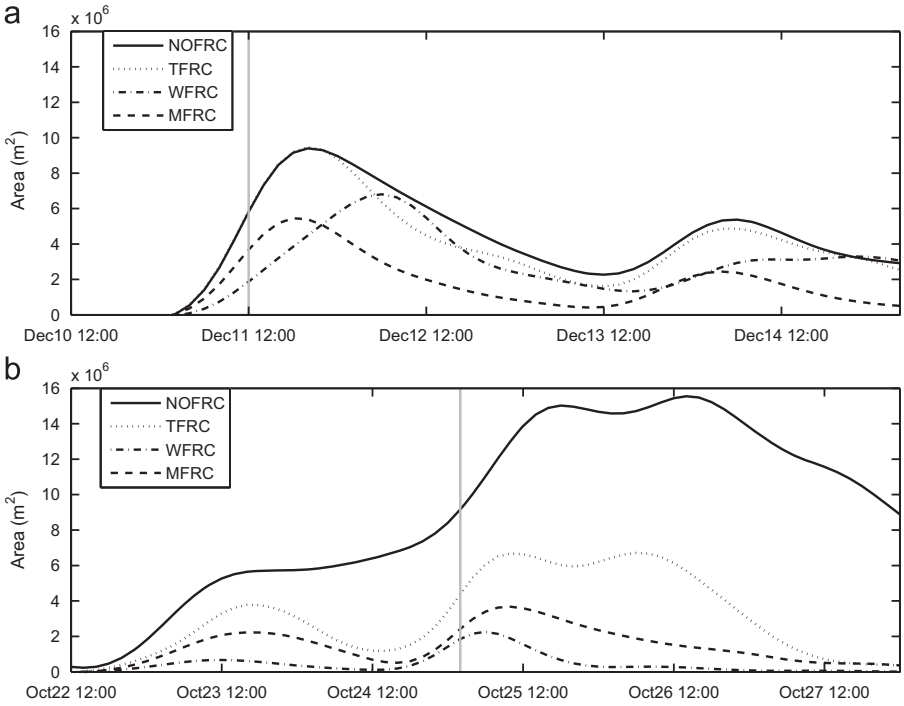

Fig. 2. Surface area of plume above the health advisory limit for different model cases for Event 1 (a) and Event 2 (b). The gray line signifies when the peak plume occurred from the mouth of the Ala Wai Canal. Date and time is in HST.

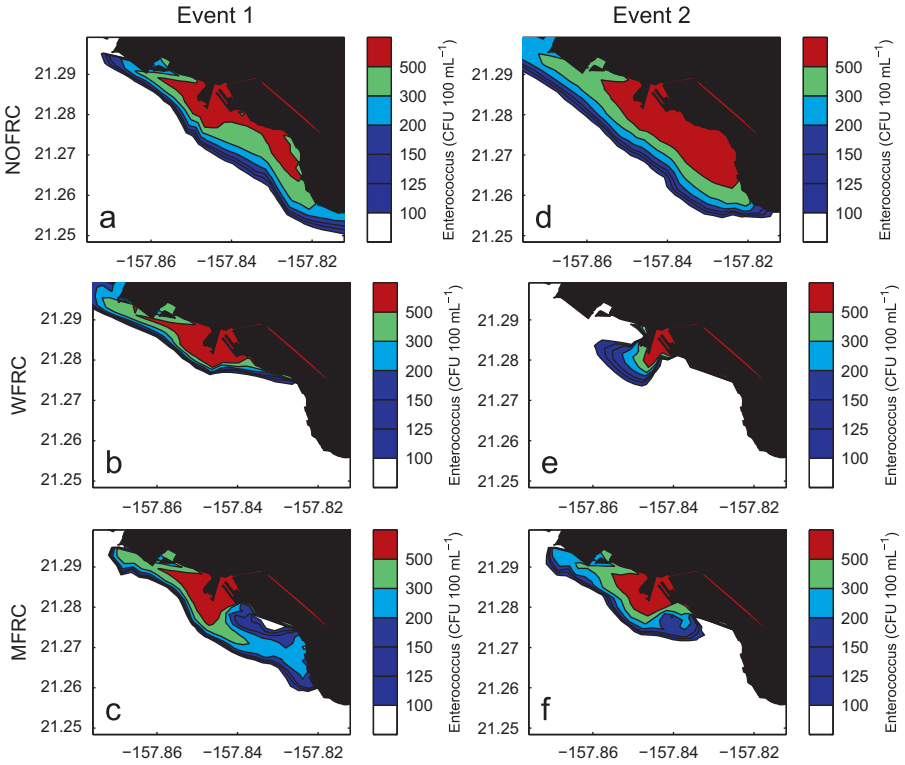

Fig. 3. Effluent plume above health advisory limit for an average computed from when the peak plume occurred until 24 h later to show the general surface area and region the plume encompassed. Column 1 is Event 1; (a) is the NOFRC case, (b) is the WFRC case, and (c) is the MFRC case. Column 2 is Event 2; (d) is the NOFRC case, (e) is the WFRC case, and (f) is the MFRC case.

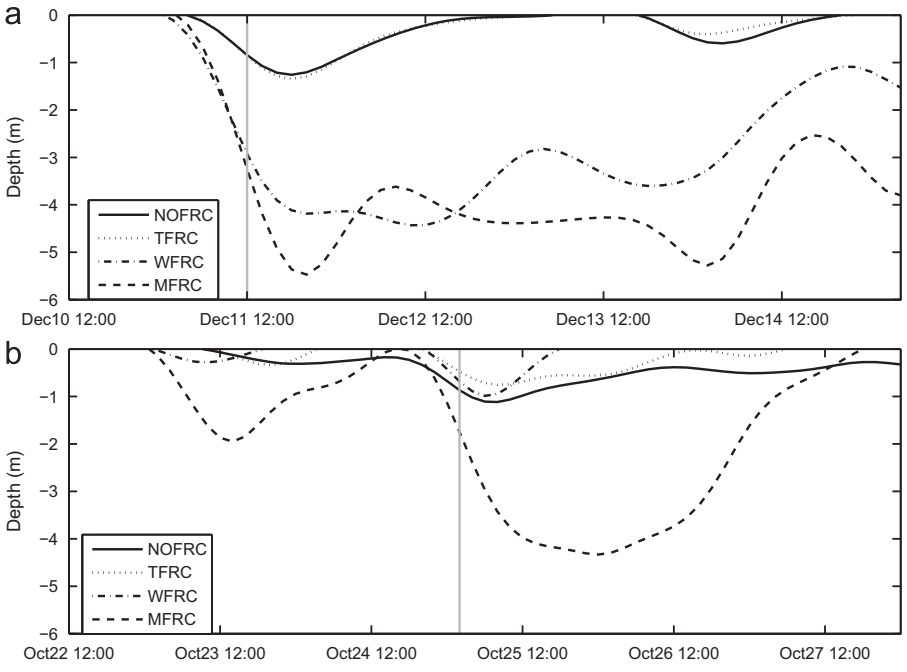

Fig. 4. Maximum depth of plume above the health advisory limit for different model cases for Event 1 (a) and Event 2 (b). The gray line signifies when the peak plume occurred from the mouth of the Ala Wai Canal. Date and time is in HST.

west forcing the plume towards Ala Moana Beach Park (Fig. 3f). Wave forcing mixed the plume to depths of almost 4.5 m in the deep swimming area fronting the park. It is important to consider the depth of the plume because *Enterococcus* spp. may persist longer at depths where UV irradiation is weaker.

To help understand the temporal evolution of the plume mass, we examined the transport of *Enterococcus* spp. out of the canal in both alongshore and cross-shore directions. We examined offshore transects both 1200 m west and east and extending 800 m offshore. A third transect connects the offshore points to measure

the cross-shore transport (see the red lines in Fig. 1). The *Enterococcus* spp. transport V_{entero} is calculated using (adapted from Choi and Wilkin, 2007):

$$V_{entero} = \int \int_{-H}^{\eta} \left(1 - \left(\frac{E_0 - E}{E_0}\right)\right) u \, dz \, dx \tag{4}$$

where η is the sea surface height anomaly, H is depth, E_0 is the background *Enterococcus* spp. concentration used for the Manoa stream (150 nmol m^{-3}), E is local *Enterococcus* spp. concentration, and u is the horizontal velocity normal to the transect. The sum of transport across each section was computed over a 24 h period for each event to account for diurnal and semidiurnal tides (when tides were included).

For Event 1, 73% of the total transport for the NOFRC experiment was offshore, as compared to only 8% for the WFRC case (Fig. 5a). Without the wind, the plume moved almost completely offshore (as determined by the transect 800 m offshore) helping to separate itself from recreational beaches; however, when the onshore Kona winds were present, the plume persisted for five days along the beaches. The wind played an important role in the cross-shore advection of the plume because it forced the *Enterococcus* laden plume onshore (Fig. 3b). Trade winds were dominant during Event 2 and did not alter the offshore transport

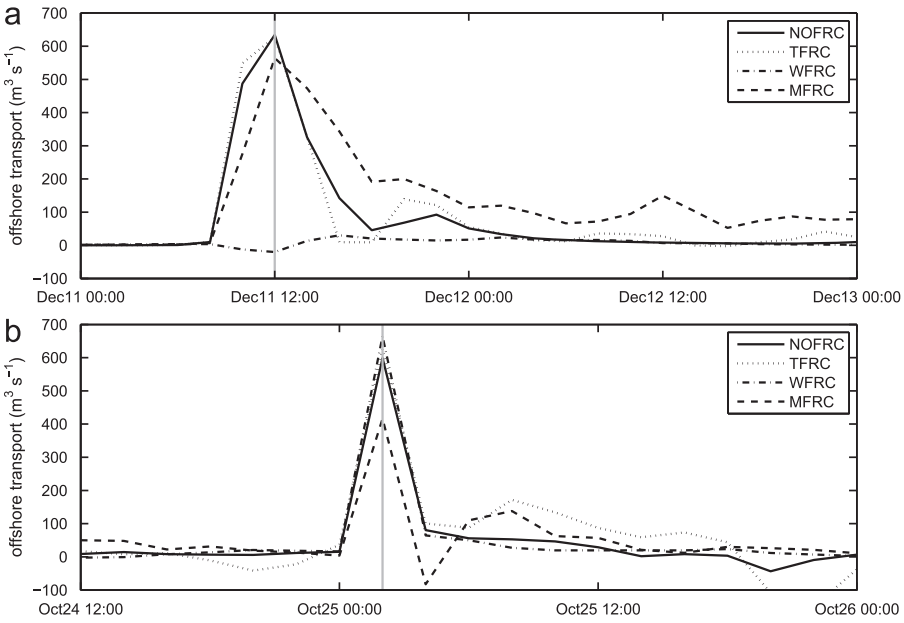

Fig. 5. Transport of *Enterococcus* spp. above the health advisory limit where positive is to the south across the offshore transect for different model cases for Event 1 (a) and Event 2 (b). The gray line signifies when the peak plume occurred from the mouth of the Ala Wai Canal. Date and time is in HST.

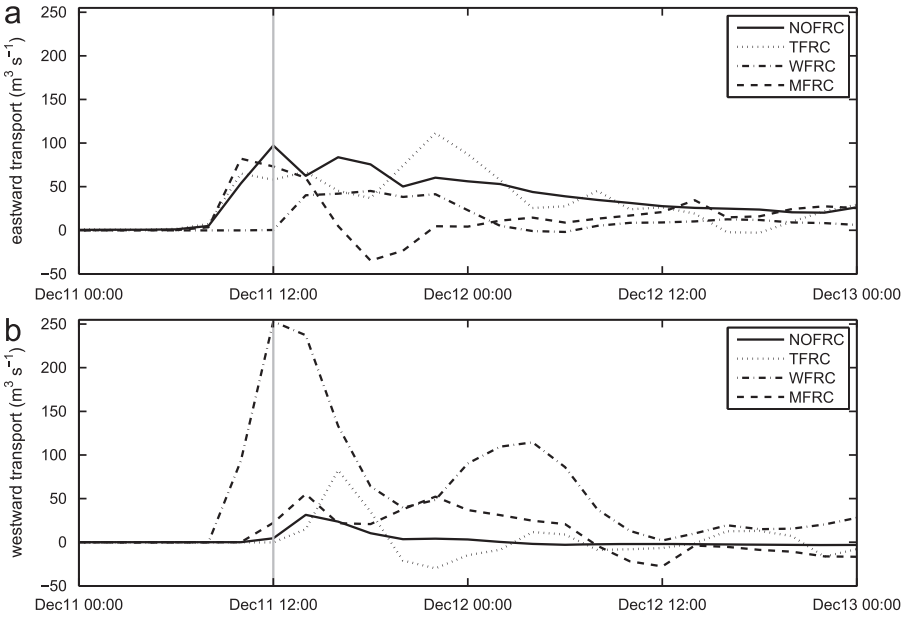

Fig. 6. Event 1 transport of *Enterococcus* spp. above the health advisory limit for different model cases across eastern and western boundaries where transports flowing across each transect away from the mouth of the canal are positive. The gray line signifies when the peak plume occurred from the mouth of the Ala Wai Canal. Date and time is in HST.

as it comprised approximately 60% of the total transport for the NOFRC and WFRC experiments (Fig. 5b). For MFRC experiments, offshore transport comprised 50% for Event 2 and almost 85% for Event 1. Although the MFRC offshore transport was less than the NOFRC for Event 2, MFRC increased offshore transport by 10–20% due to the shallow reefs on either side of the canal creating a rip current flowing out from the canal.

The transport of *Enterococcus* spp. was increased across the western section for experiments with wind and/or wave forcing (Figs. 6 and 7). For Event 1, the transport across the western section for the NOFRC experiment comprised 3% of the total transport, compared to 76% with Kona winds from the southeast forcing the plume to the northwest (Fig. 6b). The westward transport was increased by 7% for the MFRC case compared to the NOFRC case for Event 1. For Event 2, the plume stayed to the west of the mouth of the Ala Wai Canal due to the direction and magnitude of the Trade winds and waves (Fig. 3e and f). With the strong western direction of the Trade winds, there was no eastern

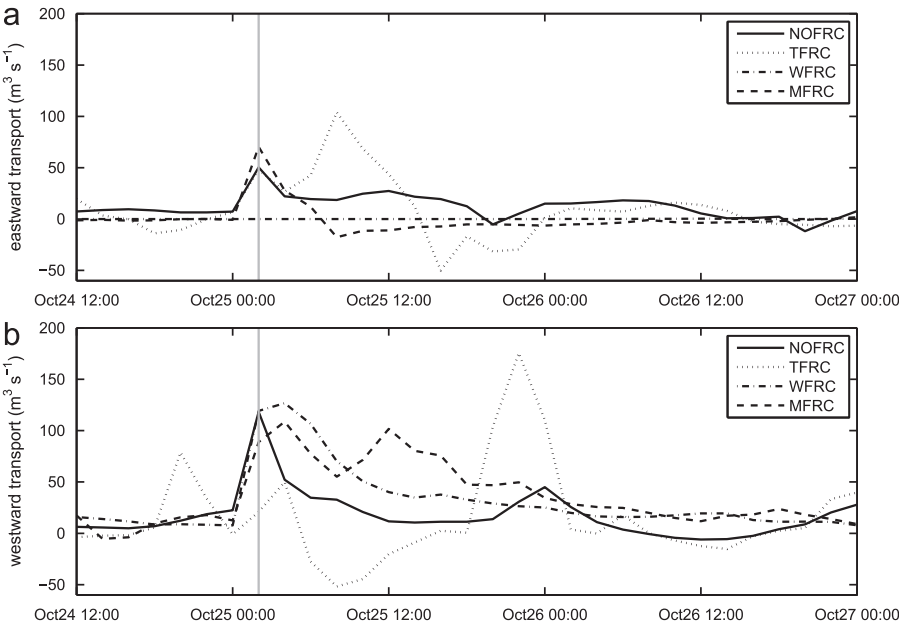

Fig. 7. Event 2 transport of *Enterococcus* spp. above the health advisory limit for different model cases across eastern and western boundaries where transports flowing across each transect away from the mouth of the canal are positive. The gray line signifies when the peak plume occurred from the mouth of the Ala Wai Canal. Date and time is in HST.

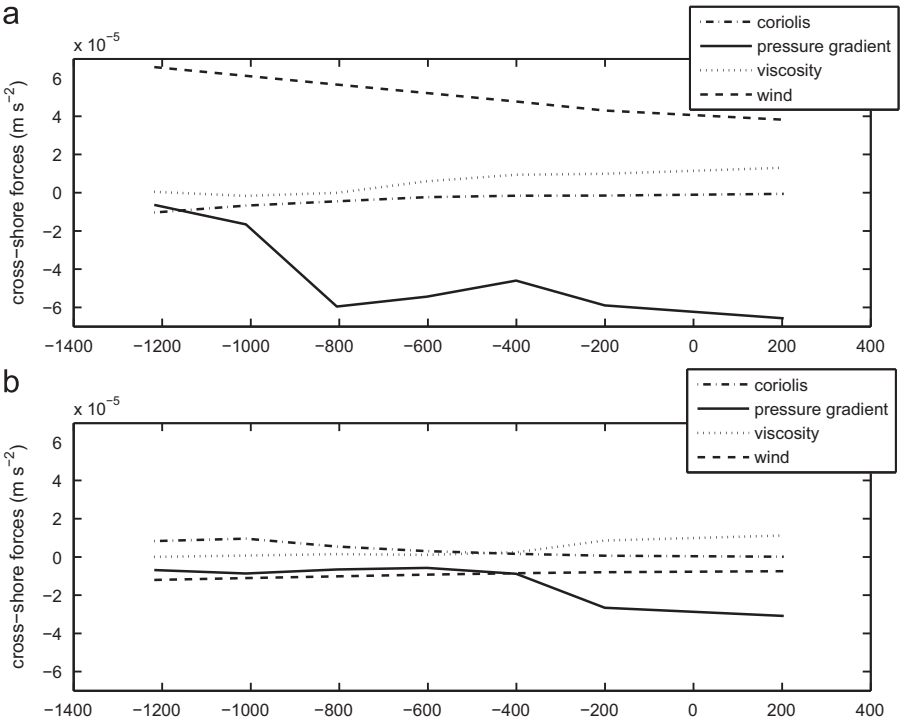

Fig. 8. Depth-integrated for the upper 2 m cross-shore momentum balance forces for a 24 h temporal mean the length of a cross-shore transect where negative is to the south of the mouth of the Ala Wai Canal, located at zero, and positive is to the north within the canal for the WFRC experiment for Event 1 (a) and Event 2 (b).

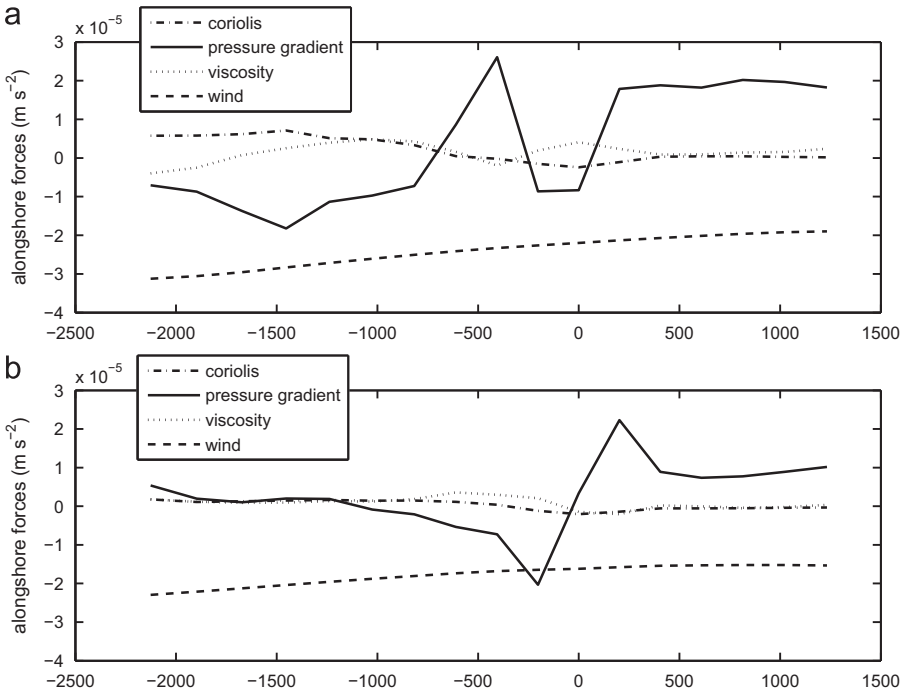

Fig. 9. Depth-integrated for the upper 2 m alongshore momentum balance forces for a 24 h temporal mean the length of an alongshore transect where negative is to the west of the mouth of the Ala Wai Canal, located at zero, and positive is to the east of the mouth for the WFRC experiment for Event 1 (a) and Event 2 (b).

transport for the WFRC experiment and 2% for the MFRC experiment compared to 15% for the NOFRC experiment (Fig. 7a). Transport across the western section made up 25% of the total transport for the NOFRC case, 40% for the WFRC case, and 50% for the MFRC case (Fig. 7b). To the east of the mouth of the canal there is shallow reef causing setup of incoming waves. Once the water has piled in this region, the plume flushes to the west increasing the amount of westward transport for experiments with wave forcing (Fig. 3c and f).

To quantify the effects of the physical forcing on the plume, we examined the average individual contributions to the momentum equation for the 24 h around the peak plume as shown in Fig. 8. For cross-shore momentum balance terms, positive is onshore and negative is offshore. For alongshore momentum balance terms, positive is to the east and negative is to the west.

Vertical sections of the cross-shore momentum balance terms were analyzed for an alongshore transect (see alongshore blue line in Fig. 1). For Event 2, stronger Trade winds began on the 23 October and persisted for more than two days. The plume experienced an Ekman force with a positive Coriolis causing a 15 cm s^{-1} increase in the westward alongshore current. For Event 1, Kona winds were variable and did not persist for more than two days; therefore, the alongshore current did not experience an increase due to Ekman forcing.

To further examine the mixing of the plume by wind and/or wave forcing, vertical sections along a cross-shore transect for alongshore momentum balance terms were analyzed (see cross-shore blue line in Fig. 1). The vertical advection for both events was weak for experiments without wave forcing within the upper 2 m; however, with wave forcing the vertical advection within the upper 5 m was more than twice as strong. Although Kona winds caused mixing of the plume within the deep lagoon, the plume was mostly constrained within the first two meters for experiments with wind forcing.

Because the majority of the plume remained near the surface, we examined depth-integrated momentum balance terms for the upper 2 m. The cross-shore momentum balance terms for both events along a cross-shore transect that extends from 200 m within the Ala Wai Canal to 1200 m offshore were examined. For the Event 1 WFRC experiment, Kona winds created an onshore wind force balanced by an offshore pressure gradient (Fig. 8a). For Event 2 WFRC, the offshore wind force due to Trade winds was balanced by a positive Coriolis force (Fig. 8b). MFRC experiments for both events exhibited an onshore pressure gradient balanced by an offshore surface radiation force.

Alongshore momentum balance terms were analyzed for a transect that extends approximately 2000 m to the west of the mouth of the Ala Wai Canal and 1000 m to the east. For both events, due to the additional mass of freshwater near the mouth of the Ala Wai Canal, a pressure gradient anomaly was set up such that to the west of the mouth the pressure gradient force was to the west, and to the east of the mouth the pressure gradient force was to the east (Fig. 9). For Event 2, the strong westerly component of the Trade winds overcame the easterly pressure gradient pushing the plume to the west of the mouth of the Ala Wai towards Ala Moana Beach Park (Fig. 9b). The variable Kona winds were not able to overcome the easterly pressure gradient allowing some of the plume to disperse both to the west and the east (Fig. 9a). MFRC experiments experienced a balance between the pressure gradient, radiation force, and bottom stress in the alongshore momentum balance.

Collectively over the five modeled events, surface area patterns were similar in that NOFRC and TFRC cases experienced the largest surface areas with significant decrease for the WFRC and MFRC cases. The maximum depth of the plume was the greatest for all events with maximum wave forcing. Offshore transport was decreased for events with Kona winds and westward transport was increased for events with Trade winds. In the cross-shore momentum balance for events with Kona winds, the onshore wind component was balanced by an offshore pressure gradient. For events with Trade winds, the offshore wind force was balanced by a positive Coriolis force. In the alongshore momentum balance, the increased sea surface height at the

mouth of the Ala Wai Canal was balanced by a westerly pressure gradient to the west of the mouth of the Ala Wai Canal and an easterly pressure gradient to the east of the mouth.

3.2. Light effects on plume

The fully coupled model with all physical forcing and the *Enterococcus* biological model was used to investigate the fate of the harmful bacteria within the plume itself and to understand how physical forcing and light influences the extent and duration of harmful bacteria contained in the plume. We examined the plume of *Enterococcus* spp. contaminated waters from the Ala Wai Canal for the five different rain events and compared the modeled concentrations to local water quality measurements. Water quality samples were collected by the City and County of Honolulu during or shortly after each of the five events. Three shoreline stations shown on Fig. 1 Ala Moana (AM), Magic Island (MI), and Waikiki (WK) and four offshore stations (C1, C2, C3, C4) were chosen to compare with model data. Water quality samples were taken by hand at the surface so model output was sampled from the upper layer for cases WTFRC, WTAFRC, and WTMFRC (abbreviations defined in Table 1).

First, we compared modeled *Enterococcus* spp. concentrations with and without inactivation from solar radiation at shoreline stations for both events. UV irradiation inactivates *Enterococcus* spp. causing a significant decrease in concentration. For Event 1, maximum concentrations occurred during the afternoon on 11 December with a peak plume in the morning allowing UV inactivation to begin earlier than seen for Event 2 (Fig. 10). *Enterococcus* spp. concentrations were reduced by approximately 50% at stations WK and MI and by 30% at station AM when considering UV inactivation; however, concentrations were still three times above the 100 CFU 100 mL^{-1} limit at all stations. For the WTFRC and WTMFRC cases at station WK, concentrations were above the limit for 4 h, then dropped below the limit for 4 h, and then exceeded the limit again due to tidal oscillations. Maximum waves reduced the time above the limit by 4 h. The waves act to both disperse (mix) the bacteria and sequester it away from the light, and the dispersal effect acts to keep the concentration below the limit for this case. For the WTAFRC case, concentrations were over the limit for 16 h at station WK; therefore, the combination of tidal oscillations, Kona winds, and average southwest swell conditions resulted in *Enterococcus* spp. concentrations exceeding water quality standards.

Modeled *Enterococcus* spp. concentrations were above the health advisory limit for stations to the west of the Ala Wai Canal (AM and MI) immediately following the peak plume for all cases as a result of Kona winds, a flood tide, and waves forcing the plume to the west. Station AM is farther west than MI, so concentrations were above the limit 2 h after the peak streamflow; whereas, concentrations were above the limit at station MI immediately following the peak streamflow. For both stations, AM and MI, concentrations peaked in the afternoon on 11 December for all cases, decreased due to inactivation, and began increasing at night as continual streamflow added *Enterococcus* spp., reaching maximum concentrations during the early morning of 12 December (Fig. 10a). Concentrations remained above the limit for 14 h on 12 December for station MI for the WTFRC case and 10 h for the WTAFRC and WTMFRC cases. At station AM, concentrations were above the limit for 12 h for the WTFRC and WTAFRC cases, and for 8 h for the WTMFRC case. When surface waves were included in the model, the amount of time *Enterococcus* spp. concentrations remained above the health advisory limit was reduced by 4 h.

The peak plume for Event 2 occurred at night with maximum *Enterococcus* spp. concentrations early the following morning for all stations. Because the peak plume occurred in the absence of solar radiation, maximum concentrations were initially similar for model runs with and without UV inactivation (Fig. 10b). Without waves, concentrations remained below the health advisory for all stations. As a result of vertical mixing when including waves, *Enterococcus* spp. concentrations were above the threshold for almost all stations because UV inactivation of *Enterococcus* spp. was reduced. Model concentrations surpassed the threshold at all stations beginning early in the morning for the WTAFRC case and remained above the

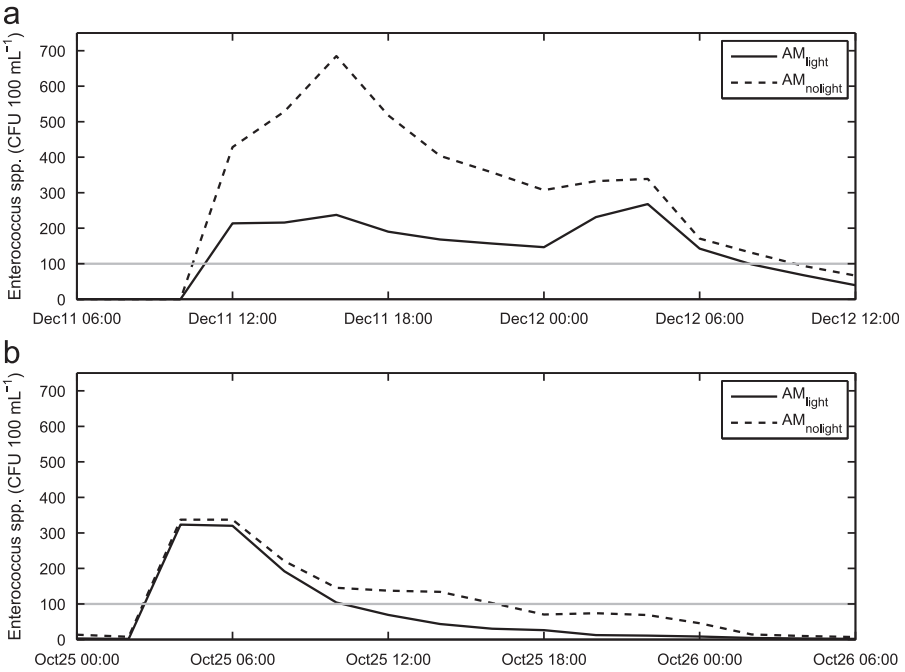

Fig. 10. Non-inactivated (no light) compared to inactivated (light) model *Enterococcus* spp. concentrations at station AM for the WTMFRC experiments for Event 1 (a) and Event 2 (b).

threshold for 6 h. For the WTMFRC case, maximum model *Enterococcus* spp. concentrations occurred one (MI) to three (AM) hours after the plume began and were three times above the limit. Six hours later, concentrations decreased and were below the limit. Concentrations remained below the limit at station WK because waves forced the plume to the west away from the station.

Modeled *Enterococcus* spp. concentrations may not fully represent observed concentrations for four primary reasons. First, the background concentration of *Enterococcus* spp. in Manoa–Palolo Stream was set as a constant based on few samples that have been taken; however, concentrations can vary particularly as a result of "first-flush effects" (discussed later). Second, the attenuation coefficient was measured in tropical seawater, not a turbid freshwater plume like that flowing out of the Ala Wai Canal. Thus, modeled UV irradiation was able to penetrate deeper into the plume, causing concentrations to be lower in the model versus observational data. Third, non-point source surface runoff into Mamala Bay likely contributed to *Enterococcus* spp. abundance not accounted for in the model. Fourth, we did not model actual wave conditions for each event, relying upon the characteristic average and maximum waves.

The covariance among all seven shoreline and offshore stations was computed using modeled *Enterococcus* spp. concentrations from all events and a six year time series of observed *Enterococcus* spp. concentrations. For both the model and the observations, there was a strong covariance between shoreline stations; however, there is no covariance between the shoreline and offshore stations. Therefore, the plume from the Ala Wai Canal as modeled and observed did not reach offshore stations and was constrained nearshore. Observed *Enterococcus* spp. concentrations at offshore stations showed evidence of contamination, which were likely from the Sand Island Outfall and not connected to the Ala Wai.

To evaluate the correlation between predicted (model) and observed (water quality) *Enterococcus* spp. concentrations, scatter plots were made. Significance tests were defined by the 95% confidence interval threshold unless otherwise noted. Model fits were performed on all available water quality data against corresponding model results (via linear time and space interpolation). Filled circles represent predicted values with concentrations below the observed assay detection limit of 1 CFU 100 mL^{-1} and open circles represent predicted values above the assay limit. For shoreline stations, we found that the model correlates well with the observations for predictions greater than the assay limit and correlates poorly with the observations when below the limit. The model consistently underestimates concentrations below the assay limit suggesting that there are other sources of water contamination when there is little to no plume from the Ala Wai Canal. However during high plume events, the Ala Wai effluence dominates the water quality. With all five plume events and all shoreline stations included, the WTFRC case showed the highest correlation to observed *Enterococcus* spp. concentrations ($R^2=0.1471$), but when the WK station was removed, the correlation improved significantly ($R^2=0.4531$) (Fig. 11). This suggests that contamination at the WK station is not from the Ala Wai Canal effluent plume, but from other non-point source runoff. The observed covariances show the weakest connection between the WK and other shoreline stations suggesting (along with the model results) that rain events control the WK station (as with the Ala Wai), but the Ala Wai and WK are only weakly connected. For offshore stations, most concentrations fell below the assay detection limit, showing again that the Ala Wai plume was constrained nearshore.

Waves had the most significant effect on the persistence of *Enterococcus* spp. by minimizing UV inactivation. Observations at the Kilo Nalu Observatory, located approximately 2 km west of the Ala Wai Canal (Fig. 1), showed a significant wave height

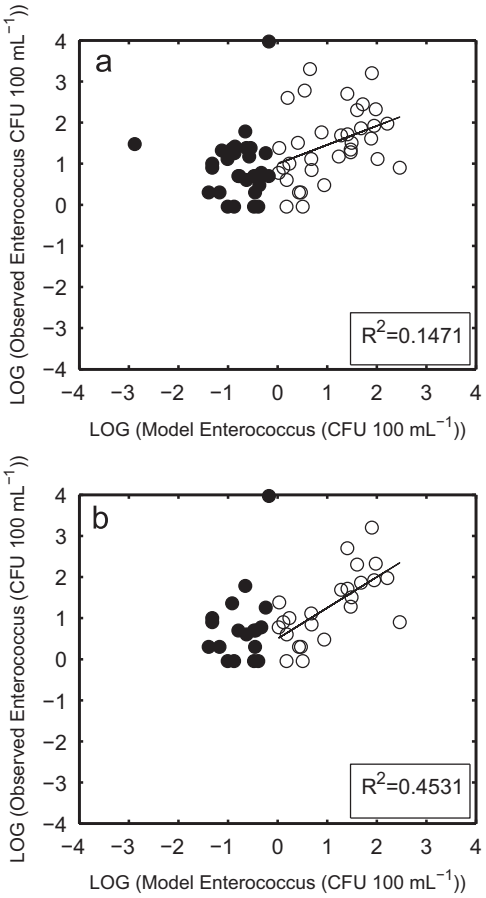

Fig. 11. Scatter plots of modeled (*x*-axis) versus observed (*y*-axis) *Enterococcus* spp. concentrations for all five events for the WTFRC case for MI, AM, and WK stations (a) and for MI and AM stations (b). Closed circles represent predicted (model) values below the assay detection limit (1 CFU 100 mL^{-1}) and open circles represent predicted (model) values above the assay detection limit.

of 3 m during Event 1 with a period of 9 s from 193° that is similar to the modeled maximum swell conditions (WTMFRC). Water quality samples were collected at stations MI, AM, WK and in the Ala Wai Canal (AW) approximately 20 h after the peak plume occurred for Event 1. *Enterococcus* spp. concentrations sampled in the Ala Wai Canal were recorded as high as 2700 CFU 100 mL^{-1} even 20 h after the event started and model values reached concentrations of 2500 CFU 100 mL^{-1} at the same period. For the WTFRC case, modeled *Enterococcus* spp. concentrations were low (89.3 and 52.7 CFU 100 mL^{-1}) for stations MI and WK and high for station AM (181.2 CFU 100 mL^{-1}) when compared to water quality data sampled on the morning of 12 December 2008. Model concentrations from the WTMFRC case were in agreement with water quality data at station MI and AM, but dropped off too quickly to compare well to station WK. This further suggests that underestimates of concentrations at station WK are from non-point source surface runoff in this area.

The contribution of non-point source surface runoff to Mamala Bay depends on weather conditions prior to a rain event. During a period of low rainfall, *Enterococcus* may accumulate resulting in increased concentrations when mobilized by a rainfall event, a phenomenon known as "first-flush effect". Because the streamflow was below the mean base flow of 0.16 m^3 s^{-1} prior to Event 1, a first-flush effect likely occurred (Tomlinson et al., 2011). This contributed to underestimates of *Enterococcus* spp. concentrations in the model. Because of the slightly increased streamflow that occurred two days before the peak streamflow, Event 2 did not experience a first-flush effect.

4. Conclusions

The physical forcing of ambient circulation, tides, winds, and surface waves affect the surface area, depth, direction, and distance offshore of the Ala Wai Canal plume during rain events. The plume from the Ala Wai Canal is a freshwater plume that is well-stratified as a surface lens and advected by the ambient circulation creating large surface areas. Tidal forcing does not cause significant mixing, allowing the plume to oscillate alongshore and offshore increasing the plume surface area. The plume is affected by seasonal wind patterns with Trade winds dominating most of the year, but Kona winds may be present during the months of October–April. Trade winds force the Ala Wai plume to the west, while Kona winds push the plume onshore and to the west. In the cross-shore momentum balance, Trade winds are balanced by the Coriolis force, while Kona winds are balanced by an offshore pressure gradient. Strong winds blowing during the beginning of a plume event will mix the plume to greater depths. If there are south-southwest swell conditions during a plume event from the Ala Wai Canal, the surface area of the plume will decrease as waves cause the plume to mix deeper and stay near-shore. The depth at which the plume is mixed is significant as UV irradiation is the main cause of inactivation in *Enterococcus* spp.; therefore, wind and waves act to sequester *Enterococcus* spp. away from the light. Although the plume behavior between average and maximum wave forcing were minor, the effect of solar radiation amplified these differences.

With zero covariance between shoreline and offshore stations, model and water quality data showed that the combined forcings act to segregate the nearshore plume from offshore. The model well represented the plume from the Ala Wai Canal during rain events at shoreline stations with the exception of Waikiki; however, when there was no plume the model poorly reflected observations everywhere, likely because the relative importance of other sources of contamination becomes more important under low flow conditions. The times and places of discrepancy between the model and observations provide useful clues about where and when the Ala Wai plume is the primary concern for water quality and where other sources need to be considered. These discrepancies are also helpful in highlighting where improvements can be made in the model to make it more generally useful.

Diagnostic models such as the one presented here are intended to complement traditional water quality sampling programs by offering enhanced spatial coverage and improved frequency. Water quality observations are an essential public health service, but the need for physical sample collections and the laboratory methods employed severely restrict the number of sites that can be monitored and result in time-lags in the reporting of results. With additional development and testing, coupled biophysical models like the one presented here can be used to generate continuous real-time predictions of water quality that will be invaluable for guiding targeted sampling for verification. This can result in more efficient use of resources and more timely public health advisories.

Acknowledgments

Stream data was provided by Heather Jeppesen at USGS. Bathymetry data of Ala Wai was provided by Jennifer Patterson. The ADCP data was provided by Sea Engineering. The data from Kilo Nalu was provided by Judith Wells. The WRF model data was provided by Yi-Leng Chen of the University of Hawaii at Manoa. The authors thank Ivica Janekovic of the Ruder Boskovic Institute for his assistance in the model runs. Ms. Johnson was supported by NOAA grant NA07NOS4730207. Dr. Powell and Ms. Johnson were supported by ONR grant N00014-09-10939. Dr. Steward was supported by NSF grant OCE08-26650 and NOAA Sea Grant NA09OAR4171048. This is SOEST publication number 8740.

References

Alford, M.H., Gregg, M.C., Merrifield., M.A., 2006. Structure, propagation, and mixing of energetic baroclinic tides in Mamala Bay, Oahu, Hawaii. Journal of Physical Oceanography 36 (997–1), 018.

Barron, C.N., Kara, C.A., Martin, P.J., Rhodes, R.C., Smedstad., L.F., 2006. Formulation, implementation and examination of vertical coordinate choices in the Global Navy Coastal Ocean Model (NCOM). Ocean Modeling 11, 347–375.

Berdeal Garcia, I., Hickey, B.M., Kawase, M., 2002. Influence of wind stress and ambient flow on a high discharge river plume. Journal of Geophysical Research 107, 3130.

Carter, G.S., Merrifield, M.A., Becker, J.M., Katsumata, K., Gregg, M.C., Luther, D.S., Levine, M.D., Boyd, T.J., Firing, Y.L., 2008. Energetics of M2 barotropic-to-baroclinic tidal conversion at the Hawaiian Islands. Journal of Physical Oceanography 38, 2,205–2,223.

Choi, Byoung-Ju, Wilkin, J.L., 2007. The effect of wind on the dispersal of the Hudson River plume. Journal of Physical Oceanography 37, 1878–1897.

Connolly, J.P., Blumberg, A.F., Quadrini, J.D., 1999. Modeling fate of pathogenic organisms in coastal waters of Oahu, Hawaii. Journal of Environmental Engineering 125, 398–406.

Davies-Colley, R.J., Bell, R.G., Donnison, A.M., 1994. Sunlight inactivation of enterococci and fecal coliforms in sewage effluent diluted in seawater. Applied and Environmental Microbiology 60, 2049–2058.

Eich, M.L., Merrifield, M.A., Alford, M.H., 2004. Structure and variability of semidiurnal internal tides in Mamala Bay, Hawaii. Journal of Geophysical Research 109, C05010, http://dx.doi.org/10.1029/2003JC002049.

Egbert, D., Bennett, F., Foreman, G.G., 1994. TOPEX/POSEIDON tides estimated using a global inverse model. Journal of Geophysical Research 99, 24,821–24,852.

Fairall, C.W., Bradley, E.F., Rogers, D.P., Edson, J.B., Young, G.S., 1996. Bulk parameterization of air-sea fluxes for tropical ocean-global atmosphere coupled-ocean atmosphere response experiment. Journal of Geophysical Research 101, 3747–3764.

Fong, D.A., Geyer, W.R., 2001. Response of a river plume during an upwelling favorable wind event. Journal of Geophysical Research 106, 1067–1084.

Garvine, R.W., 1987. Estuary plumes and fronts in shelf waters: a layer model. Journal of Physical Oceanography 17, 1877–1896.

Garvine, R.W., 1995. A dynamical system for classifying buoyant coastal discharges. Continental Shelf Research 15, 1585–1596.

Guo, Xinyu, Valle-Levinson, A., 2007. Tidal effects on estuarine circulation and outflow plume in the Chesapeake Bay. Continental Shelf Research 27, 20–42.

Hamilton, P., J.J. Singer and E. Waddell (1995) Ocean Current Measurements. Final Report. Mamala Bay Study. Project MB-6. Mamala Bay Study Comm., Honolulu, Hawaii.

Hassen, A., Mahrouk, M., Ouzari, H., Cherif, M., Boudabous, A., Damelincourt, J.J., 2000. UV disinfection of treated wastewater in a large-scale pilot plant and inactivation of selected bacteria in a laboratory UV device. Biosource Technology 74, 141–150.

Hickey, B.M., Pietrafesa, L.J., Jay, D.A., Boicourt, W.C., 1998. The Columbia River plume study: subtidal variability in the velocity and salinity fields. Journal of Geophysical Research 103, 10,339–10,368 http://www.soest.hawaii.edu/hmrg/Multibeam/index.php, December, 2011.

Janekovic, I., Powell, B.S., 2012. Analysis of imposing tidal dynamics to nested numerical models. Continental Shelf Research 34, 30–40.

Masse, A.K., Murthy, C.R., 1992. Analysis of the Niagara River plume dynamics. Journal of Geophysical Research 97, 2403–2420.

Matthews, D., Powell, B.S., Janekovic., I., 2012. Analysis of four-dimensional variational state estimation of the Hawaiian waters. Journal of Geophysical Research 117, C03013.

Natarov, A., Powell., B.S., 2012. Sensitivity of the Hawaiian Lee Counter Current to winds and upstream conditions. Dynamics of Atmospheres and Oceans, in revision, 2012.

O'Donnell, J., 1990. The formation and fate of a river plume: a numerical model. Journal of Physical Oceanography 20, 551–569.

Orton, P.M., Jay, D.A., 2005. Observations at the tidal plume front of a high-volume river outflow. Geophysical Research Letters 32, L11605.

Parsons, R.R., Takahashi, M., Hargrave, B., 1977. Biological Oceanographic Processes. Pergamon.

Powell, B.S., Janekovic, I., Carter, G.S., Merrifield., M.A., 2012. Sensitivity of internal tide generation in Hawaii. Geophysical Research Letters 39 (1–6), 2012, L10606.

Pullen, J.D., Allen, J.S., 2000. Modeling studies of the coastal circulation off Northern California: shelf response to a major Eel river flood event. Continental Shelf Research 20, 2213–2238.

Roland, A., Cucco, A., Ferrarin, C., Hsu, T.W., Liau, J.M., Ou, S.H., Umgiesser, G., Zanke., U., 2009. On the development and verification of a 2-D coupled wave-current model on unstructured meshes. Journal of Marine Systems 78 (1), S244–S254.

Shchepetkin, A.F., McWilliams, J.C., 2005. The Regional Ocean Modeling System: a split-explicit, free-surface, topography-following-coordinate ocean model. Ocean Modeling 9, 347–404.
Tomlinson, M.S., De Carlo, E.H., McManus, M.A., Pawlak, G., Steward, G.F., Sansone, F.J., Nigro, O.D., Timmerman, R.E., Patterson, J., Jaramillo, S., Ostrander, C.E., 2011. Characterizing the effects of two storms on the coastal waters of O'ahu, Hawai'i, using data from the Pacific Islands Ocean Observing System. Oceanography 24, 182–199.
Venzon Jr., N.C., 2007. Massive discharge of untreated sewage into the Ala Wai canal (Oahu, Hawaii): a threat to Waikiki's waters? Journal of Environmental Health 0, 25–29.
Walker, N.D., 1996. Satellite assessment of Mississippi River plume variability: causes and predictability. Remote Sensing: Environment 58, 21–35.
Whitney, M.M., Garvine, R.W., 2006. Simulating the Delaware Bay buoyant outflow: comparison with observations. Journal of Physical Oceanography 36, 3–21.
Wiseman Jr., W.J., Garvine, R.W., 1995. Plumes and coastal currents near large river mouths. Estuaries 18, 509–517.
Xie, S.P., Liu, W., Liu, Q., Nonaka., M., 2001. Far-reaching effects of the Hawaiian Islands on the Pacific Ocean-Atmosphere System. Science 292 (5524), 2057–2060.